HHS Public Access

Author manuscript

Nature. Author manuscript; available in PMC 2012 October 26.

Published in final edited form as:

Nature. ; 484(7395): 529–533. doi:10.1038/nature10975.

Exploiting a natural conformational switch to engineer an Interleukin-2 superkine

Aron M. Levin[1,*], **Darren L. Bates**[2,*], **Aaron M. Ring**[2,*], **Carsten Krieg**[3,4,*], **Jack T. Lin**[5], **Leon Su**[5], **Ignacio L. Moraga**[2], **Miro E. Raeber**[3,4], **Gregory R. Bowman**[6], **Paul Novick**[6], **Vijay S. Pande**[6], **C. Garrison Fathman**[5], **Onur Boyman**[3,4,†], and **K. Christopher Garcia**[1,2,†]

[1]Howard Hughes Medical Institute, Stanford University School of Medicine, Stanford, CA 94305, USA [2]Department of Molecular and Cellular Physiology, and Department of Structural Biology, Stanford University School of Medicine, Stanford, CA 94305, USA [3]Laboratory of Applied Immunobiology, University of Zurich, Zurich, CH-8006, Switzerland [4]Allergy Unit, Department of Dermatology, University Hospital Zurich, Zurich, CH-8091, Switzerland [5]Stanford University School of Medicine, Department of Medicine, Division of Immunology and Rheumatology, Stanford, CA 94305, USA [6]Department of Chemistry, Stanford University, Stanford, CA 94305, USA

Abstract

The immunostimulatory cytokine interleukin-2 (IL-2) is a growth factor for a wide range of leukocytes, including T cells and natural killer (NK) cells[1–3]. Considerable effort has been invested using IL-2 as a therapeutic agent for a variety of immune disorders ranging from AIDS to cancer. However, adverse effects have limited its use in the clinic. On activated T cells, IL-2 signals through a quaternary “high affinity” receptor complex consisting of IL-2, IL-2Rα (termed CD25), IL-2Rβ, and γ_c[4–8]. Naïve T cells express only a low density of IL-2Rβ and γ_c, and are therefore relatively insensitive to IL-2, but acquire sensitivity after CD25 expression, which captures the cytokine and presents it to IL-2Rβ andγ_c. Here, using *in vitro* evolution, we eliminated IL-2’s functional requirement for CD25 expression by engineering an IL-2 “superkine” (termed super-2) with increased binding affinity for IL-2Rβ. Crystal structures of super-2 in free and receptor-bound forms showed that the evolved mutations are principally in the core of the

†To whom correspondence should be addressed. kcgarcia@stanford.edu (K.C.G.) or onur.boyman@uzh.ch (O.B.).
*These authors contributed equally to this work

Author Contributions A.L. performed in vitro evolution and contributed to preparation of manuscript. D.L.B. produced recombinant proteins, determined crystal structures, and carried out surface plasmon resonance analysis. A.M.R. carried out cellular and signaling assays, biophysical measurements, and contributed to preparation of the manuscript. C.K. carried out *in vivo* experiments, analyzed data, and contributed to preparation of the manuscript, M.E.R. carried out *in vivo* experiments in mice. I. M. analyzed cell signaling data. G.R.B., P.N., and V.S.P. carried out and analyzed molecular dynamics simulations. J.T.L., L.S., and C.F.G. performed and analyzed T cell signaling experiments. O.B. designed and supervised *in vivo* experiments, analyzed data and contributed to preparation of manuscript. K.C.G conceived of project, analyzed data, supervised execution of project, and prepared the manuscript.

Author Information Atomic coordinates and structure factors for the reported crystal structures have been deposited with the Protein Data Bank under accession codes 3QAZ and 3QB1. K.C.G., A.L., and A.R. declare competing financial interests due to submission of a pending patent application describing super-2. O.B. declares competing financial interests due to being a shareholder of Nascent Biologics Inc..

cytokine, and molecular dynamics simulations indicated that the evolved mutations stabilized IL-2, including a flexible helix in the IL-2Rβ binding site, into an optimized receptor-binding conformation resembling that when bound to CD25. The evolved mutations in super-2 recapitulated the functional role of CD25 by eliciting potent phosphorylation of STAT5 and vigorous proliferation T cells irrespective of CD25 expression. Compared to IL-2, super-2 induced superior expansion of cytotoxic T cells, leading to improved anti-tumor responses *in vivo*, and elicited proportionally less expansion of T regulatory cells and reduced pulmonary edema. Collectively, we show that *in vitro* evolution has mimicked the functional role of CD25 in enhancing IL-2 potency and regulating target cell specificity, which has implications for immunotherapy.

Results

Affinity maturation of IL-2 for IL-2Rβ

In order to engineer a CD25-independent version of IL-2, we displayed human IL-2 on the surface of yeast as a conjugate to Aga2p, and verified proper receptor binding properties with IL-2R β and γ_c ectodomain tetramers that were *C*-terminally biotinylated and coupled to phycoerythrin-conjugated streptavidin for use as a staining and sorting reagent[9,10]. Yeast-displayed IL-2 bound to γ_c in the presence of IL-2Rβ, recapitulating the cooperative assembly of the heterodimeric receptor complex as seen with soluble IL-2 (Fig. 1a, Supplementary Fig. 1). We proceeded to carry out two generations of *in vitro* evolution (Fig. 1b, Supplementary Fig. 2). Our first generation *in vitro* evolution strategy was to create an error-prone PCR library of the entire IL-2 coding sequence (Supplementary Fig. 2), which resulted in selection of a predominant IL-2 variant containing an L85V mutation (Fig 1c, Supplementary Fig. 3).

From inspection of the wild-type (WT) IL-2 structure, we were surprised to find that position 85 was not a direct IL-2Rβ contact residue, but rather resided on the internal face of the IL-2 C-helix, within the hydrophobic core of the cytokine (Fig. 2a). Thus, we surmised that L85V may affect the structure of helix C in a way that enhances binding to IL-2Rβ. Therefore, we carried out a second generation selection where we made a biased library that contained F/I/L/V at amino acids L80, L85, I86, I89, I92, and V93, which are contained within the hydrophobic core and linker region on helix C (Fig. 1b,c). To rapidly select the most active variants, we used the yeast-displayed cytokines themselves to stimulate STAT5 phosphorylation in the human NK cell line YT-1 by coincubation at varying yeast:YT-1 cell ratios (Fig 1d, Supplementary Fig. 4). Several clones stimulated substantially more STAT5 phosphorylation at lower yeast:cell ratios than yeast-displayed WT IL-2 (Fig 1d, Supplementary Fig. 4). Sequencing of a selected panel of high-affinity IL-2 clones revealed a consensus set of mutations L80F/R81D/L85V/I86V/I92F (Fig 1c, Supplementary Fig. 3).

Structure and comparison with WT IL-2

We expressed recombinant forms of several first and second-generation IL-2 clones in order to measure their binding affinities and kinetics for IL-2Rβ by surface plasmon resonance (SPR) (Fig. 1c, Supplementary Figs 3 and 5) and isothermal titration calorimetry (ITC) (Supplementary Fig. 6). By SPR, the affinity between IL-2 and IL-2Rβ was K_D = 280 nM.

The IL-2 superkines, termed “super-2s”, clustered into low, medium, and high affinity classes. The highest affinity mutants had K_Ds of 1.2–1.7 nM (D10, H9). The affinity increases were uniformly manifested in reductions in off-rates (Fig 1c, Supplementary Figs 3 and 5).

In order to understand the structural consequences of the evolved mutations, we crystallized the D10 super-2 (Fig. 2a, Supplementary Fig. 7a, and Supplementary Table 1). In the structure of D10 alone, five of the six mutations clustered on the B-C loop and within the C-helix core, in positions that did not contact IL-2Rβ. Notably, the B-C-helix linker region was ordered in the electron density map (Supplementary Figs 7a and 8a), compared to other IL-2 structures where this region is often disordered (Supplementary Fig. 8a). Collectively, the F80, V85, and V86 substitutions appeared to collapse into a hydrophobic cluster that stabilized the loop by pinning the C-helix into the core of the molecule. Only one of the five consensus mutations, I92F, was at a position that contacted IL-2Rβ in the receptor complex (Fig. 2a), but it was deeply inserted between the C and A helices, contributing only an additional 10Å^2 of molecular surface buried by IL-2Rβ in the complex compared to Ile92. We also determined a low-resolution (3.8 Å) structure of the D10 ternary receptor complex to assess whether the mutations have perturbed the IL-2Rβ/γ_c receptor dimer geometry compared to the WT IL-2 complex (Fig. 2b, Supplementary Table 1). The overall IL-2Rβ/γ_c heterodimeric architecture and mode of cytokine/IL-2Rβ contact in the D10 ternary complex were essentially identical to the previously reported IL-2 quaternary assembly (RMSD = 0.43 Å) (Supplementary Fig. 7b).

Previously, we found that the C-helix of IL-2 appears to undergo subtle repositioning upon binding to IL-2Rα[11] (Fig. 2c, Supplementary Fig. 8a). Inspection of three WT unliganded IL-2 structures revealed conformational variability in the C-helix position, consistent with higher crystallographic B-factors in this helix relative to the rest of the molecule (Supplementary Fig. 8b). We compared the structure of our D10 super-2 to that of an unliganded structure of IL-2, and IL-2 in the receptor complexes. We found that the C-helix in D10 was more similar to that seen in the two receptor-bound conformations of IL-2 than the free forms, having undergone a relatively small shift towards the helical core as a consequence of the stabilizing mutations (Fig. 2c).

We used molecular dynamics (MD) simulations of IL-2 and D10 to further interrogate the mechanism responsible for higher binding affinity to IL-2Rβ by super-2 (Fig. 2d,e). We constructed an atomically detailed Markov state model (MSM) in order to directly probe the relative conformational flexibility of IL-2 versus D10. Analysis of the MSM clearly demonstrated that D10 was more stable than IL-2, and that IL-2 visited nearly twice as many clusters as D10. For example, D10’s most populated state had an equilibrium probability of ~0.20, compared to ~0.05 for IL-2, demonstrating that D10’s equilibrium population was far more localized than IL-2. Helix B, the B-C loop, and helix C appeared rigidified in D10 compared to IL-2 as evidenced by reduced RMSD from the starting conformations (Fig. 2d, Supplementary Movies 1, 2). F92 appeared to act as a molecular wedge between helix C and helix A, stabilizing the more C-terminal end of the helix (Fig. 2a). We also simulated both D10 and IL-2 starting in a receptor-bound-like structure and monitored the divergence in RMSD of the B-C loop and helix C from the actual receptor-bound structure. IL-2 (Fig. 2e-

left, Supplementary Fig. 8c) quickly "wandered" from the receptor conformation and experienced drastic fluctuations compared to D10 (Fig. 2e-right, Supplementary Fig. 8c, Supplementary Movies 1, 2). Based on these observations, we propose a mechanism whereby the reduced flexibility of helix C in super-2, as a result of its improved core packing with helix B, results in a superior receptor-binding poise that increases its affinity for IL-2Rβ, and consequently mimics a functional role of CD25. The structural and MD results suggest that the evolved mutations in super-2 cause a conformational stabilization of the cytokine, that reduces the energetic penalties for binding to IL-2Rβ.

Stimulation of NK cells

We asked if the super-2s demonstrated signaling potencies on cells in accordance with their IL-2Rβ binding affinities, and whether their activities depended on cell surface expression of CD25. We determined the dose-response relationships of WT IL-2 versus the super-2s 6-6, D10, and H9 on both $CD25^-$ and $CD25^+$ human YT-1 NK cells by assaying STAT5 phosphorylation with flow cytometry (Fig. 3a–d, Supplementary Fig. 9). On $CD25^-$ YT-1 cells, the EC_{50} of H9 and D10 were decreased over 10-fold (EC_{50} = 2.5 and 1.8 ng/mL, respectively) compared to IL-2 (EC_{50} = 39 ng/mL), with the 6-6 mutein yielding an EC_{50} intermediate between IL-2 and H9/D10 (EC_{50} = 15 ng/mL), consistent with the improved affinity of the super-2s for IL-2Rβ (Fig. 3a). On $CD25^+$ YT-1 cells, the EC_{50} of IL-2 decreased over 50-fold relative to $CD25^-$ YT-1 cells, from 39 to 0.66 ng/mL (Fig. 3b). In contrast, the EC_{50} of H9 and D10 improved only modestly in the presence of CD25 (EC_{50} of 0.47 and 0.52 compared to 2.5 and 1.8 ng/mL, respectively) (Fig. 3b).

We sought to further probe the CD25-independence of the super-2s by taking advantage of a previously characterized mutation in IL-2, Phe42 to Ala (F42A), which showed reduced binding to CD25 by ~220-fold for H9 (K_D 6.6 nM versus 1.4 μM) and ~120-fold for IL-2 (K_D 6.6 nM versus 0.8 μM) (Supplementary Fig. 10)[12,13]. The F42A mutation is an alternative diagnostic probe of the relative CD25 dependence of IL-2 and super-2. The F42A mutation right-shifted the dose-response curve of WT IL-2 on $CD25^+$ cells by ~1 log, but had no effect on $CD25^-$ cells (Fig. 3c). In contrast, H9 was far less sensitive to the F42A mutation, with the dose-response curves of H9 versus H9 F42A being very similar on both $CD25^+$ and $CD25^-$ cells (Fig. 3d).

Activity of super-2 on T cells

We assessed the activity of several super-2s on T cells that were either deficient in, or expressed CD25. For the former experiment, $CD4^+$ T cells were isolated from CD25-knockout mice, followed by stimulation by either WT IL-2 or six super-2s and assaying for STAT5 phosphorylation at a range of cytokine concentrations (Fig 3e, Supplementary Fig. 11). $CD25^{-/-}$ $CD4^+$ T cells responded poorly to exogenous WT IL-2 stimulation, but super-2s induced STAT5 phosphorylation in these cells proportional to their affinity for IL-2Rβ.

The principle functional effect of IL-2 is to promote T cell proliferation, particularly for naïve T cells. Human naïve $CD4^+$ T cells were isolated and left either unstimulated or stimulated with plate-bound anti-CD3 antibody with or without the different IL-2 variants

(Fig 3f, Supplementary Fig. 12). Increased proliferation effects on naïve human T cells correlated with increased affinity for IL-2Rβ and STAT5 phosphorylation shown earlier, as the rank order of potency was D10 = H9 > 6-6 > WT IL-2 (see Supplementary Fig. 12 for the complete titration).

We next tested the IL-2 variants for their ability to induce STAT5 phosphorylation on experienced human $CD4^+$ T cells (Supplementary Fig. 13), which highly express the trimeric IL-2Rαβγ complex. Human $CD4^+$ T cells were *in vitro* activated by T cell receptor (TCR) stimulation and rested to generate "experienced" human $CD4^+$ $CD25^+$ T cells. As for the $CD25^+$ YT-1 cells, we observed a much smaller difference between IL-2 and the super-2s.

In vivo properties of super-2

We assessed the potency of the super-2 H9 on expansion of $CD25^{low}$ versus $CD25^{high}$ T cells, in comparison to WT IL-2 and IL-2/anti-IL-2 monoclonal antibody (mAb) complexes, which have been shown to exert reduced pulmonary edema yet very potent anti-tumor responses *in vivo*[14–16]. On antigen-experienced (memory-phenotype, MP) $CD8^+$ T cells, expressing only low levels of CD25 but high levels of IL-2Rβγ, H9 induced more than three times the rate of proliferation and expansion as WT IL-2 (Fig 4a, Supplementary Fig. 14a). However, on $CD4^+$ $CD25^{high}$ T regulatory (Treg) cells, we found that the CD25-competent WT IL-2 and H9 achieved comparable maximal expansion, demonstrating again that expression of CD25 mitigates the difference between super-2 and WT IL-2 (Fig. 4a, S14b). Thus, the H9 exhibits the desired property that it shows enhanced stimulation towards $CD8^+$ T cells, but not towards Treg cells compared to WT IL-2.

As previously reported, administration of high-dose WT IL-2 for five days induced substantial pulmonary edema, which is known to be CD25-dependent[15] (Fig. 4b). Although significantly more stimulatory for cytotoxic $CD8^+$ T cells (Fig. 4a), H9 super-2 caused substantially less pulmonary edema (Fig. 4b).

Given the more favorable properties of H9 in comparison to IL-2, we assessed its ability to stimulate effector functions of cytotoxic T cells in four different tumor models *in vivo*, where high-dose IL-2 administration has been previously shown to result in tumor regression[15,17]. To this end, C57BL/6 mice were injected subcutaneously with B16F10 melanoma cells, followed by administration of either high-dose IL-2, IL-2/anti-IL-2 mAb complexes, or H9 super-2, once tumor nodules became visible and palpable. PBS-treated control mice rapidly developed large subcutaneous tumors reaching a volume of about 1500 mm^3 on day 18 (Fig. 4c). As previously shown, high-dose IL-2 treatment was able to delay tumor growth by as much as 39% on day 18 ($p<0.05$), while IL-2/anti-IL-2 mAb complexes exerted very effective tumor control, reducing tumor growth by >80% on day 18 ($p<0.005$) (Fig. 4c). Significantly, similar to IL-2/anti-IL-2 mAb complexes, mice receiving high-dose H9 showed a dramatic decrease of tumor load on day 18, which was reduced by >80% compared to PBS ($p<0.005$) and by >70% compared to WT IL-2 ($p<0.005$) (Fig. 4c). Similar results were obtained using three other tumor models, including murine colon carcinoma and Lewis lung carcinoma injected subcutaneously (Fig. 4d,e) and B16F10 cells administered intravenously (Fig. 4f, Supplementary Fig. 15). Collectively, these data show

that the H9 super-2 is very effective against different tumors, albeit inducing reduced pulmonary edema.

The practical implications are that this conformational nuance in IL-2 can be exploited for therapy. Super-2 robustly activates cytotoxic $CD8^+$ T cells and NK cells for potent anti-tumor immune responses, yet it elicits minimal toxicity, suggesting that super-2 could warrant reconsideration for clinical applications of IL-2.

Methods Summary

Yeast display and selection of IL-2

Error-prone and site-directed libraries of IL-2 were displayed on yeast as previously described[18] and stained with biotinylated IL-2Rβ at successively decreasing concentrations. Staining was detected with streptavidin-PE and yeast were separated using paramagnetic anti-PE microbeads (Miltenyi; MACS). Enrichment of positively-staining yeast was monitored by flow-cytometry.

Protein expression, purification, and structural determination

Human IL-2 variants and the ectodomains of IL-2Rβ, γ_c, and CD25 were expressed in Hi5 cells and purified as previously described[11]. Proteins were concentrated to 8–20 mg/mL and crystallized by vapor diffusion in sitting drops. Diffraction studies were performed at the Stanford Synchrotron Radiation Laboratory and the Advanced Light Source. Crystal structures were solved by molecular replacement with PHASER[19] and refined using PHENIX[20] and COOT[21].

Mice

C57BL/6 and Thy1.1-congenic mice on a C57BL/6 background were maintained under specific pathogen-free conditions and used at 3–6 months of age. Experiments were performed in accordance with the Swiss Federal Veterinary Office guidelines and approved by the Cantonal Veterinary Office.

In vivo T cell proliferation

$2–3\times10^6$ CFSE-labeled $CD44^{high}$ $CD8^+$ T cells from Thy1.1-congenic mice were injected intravenously to Thy1.2-congenic animals. Mice received daily intraperitoneal (i.p.) injections of PBS, 20 μg IL-2, 1.5 μg IL-2/anti-IL-2 mAb complexes, or 20 μg H9 for 5 days. On the sixth day, spleens were removed and analyzed by flow cytometry.

Toxicity

Pulmonary edema was determined by measurement of pulmonary wet weight on the sixth day after five daily i.p. injections of PBS, 20 μg IL-2, 1.5 μg IL-2/anti-IL-2 mAb complexes, or 20 μg H9 as previously described[15].

Tumor models

B16F10 melanoma cells, Lewis lung carcinoma, or murine colon carcinoma 38 cells were injected into mice (3–4 mice/group), as previously reported[15,17]. Treatment consisted of five daily i.p. injections of PBS, 20 μg IL-2, 1.5 μg IL-2/anti-IL-2 mAb complexes, or 20 μg H9.

Supplementary Material

Refer to Web version on PubMed Central for supplementary material.

Acknowledgments

The authors gratefully acknowledge W. Leonard, R. Levy, and R. Schwendener for reagents and discussion. This work was supported by NIH-RO1AI51321 (to K.C.G.), PP00P3-128421 from the Swiss National Science Foundation and KFS-02672-08-2010 from the Swiss Cancer League (both to O.B.), NIH R01-GM062868 (to V.P.), MRI-R2 [This award is funded under the American Recovery and Reinvestment Act of 2009 (Public Law 111-5)] (to V.P.), NIH-AR050942 (to J.T.L.), NIH U01 DK078123 (to C.G.F.), and NIH U19 AI 082719 (to C.G.F.). A.M.R. was supported by the Stanford Medical Scientist Training Program (NIH- GM07365). K.C.G. is an Investigator of the Howard Hughes Medical Institute.

References

1. Rochman Y, Spolski R, Leonard WJ. New insights into the regulation of T cells by gamma(c) family cytokines. Nat Rev Immunol. 2009; 9 (7):480–490. [PubMed: 19543225]
2. Smith KA. Interleukin-2: inception impact, and implications. Science. 1988; 240 (4856):1169–1176. [PubMed: 3131876]
3. Waldmann TA. The biology of interleukin-2 and interleukin-15: implications for cancer therapy and vaccine design. Nat Rev Immunol. 2006; 6 (8):595–601. [PubMed: 16868550]
4. Cosman D, et al. Cloning, sequence and expression of human interleukin-2 receptor. Nature. 1984; 312 (5996):768–771. [PubMed: 6096720]
5. Leonard WJ, et al. Molecular cloning and expression of cDNAs for the human interleukin-2 receptor. Nature. 1984; 311 (5987):626–631. [PubMed: 6090948]
6. Nikaido T, et al. Molecular cloning of cDNA encoding human interleukin-2 receptor. Nature. 1984; 311 (5987):631–635. [PubMed: 6090949]
7. Hatakeyama M, et al. Interleukin-2 receptor beta chain gene: generation of three receptor forms by cloned human alpha and beta chain cDNA's. Science. 1989; 244 (4904):551–556. [PubMed: 2785715]
8. Takeshita T, et al. Cloning of the gamma chain of the human IL-2 receptor. Science. 1992; 257 (5068):379–382. [PubMed: 1631559]
9. Boder ET, Wittrup KD. Yeast surface display for screening combinatorial polypeptide libraries. Nat Biotechnol. 1997; 15 (6):553–557. [PubMed: 9181578]
10. Chao G, et al. Isolating and engineering human antibodies using yeast surface display. Nat Protoc. 2006; 1 (2):755–768. [PubMed: 17406305]
11. Wang X, Rickert M, Garcia KC. Structure of the quaternary complex of interleukin-2 with its alpha, beta, and gammac receptors. Science. 2005; 310 (5751):1159–1163. [PubMed: 16293754]
12. Mott HR, et al. The solution structure of the F42A mutant of human interleukin 2. J Mol Biol. 1995; 247 (5):979–994. [PubMed: 7723044]
13. Thanos CD, DeLano WL, Wells JA. Hot-spot mimicry of a cytokine receptor by a small molecule. Proc Natl Acad Sci U S A. 2006; 103 (42):15422–15427. [PubMed: 17032757]
14. Boyman O, Kovar M, Rubinstein MP, Surh CD, Sprent J. Selective stimulation of T cell subsets with antibody-cytokine immune complexes. Science. 2006; 311 (5769):1924–1927. [PubMed: 16484453]

15. Krieg C, Letourneau S, Pantaleo G, Boyman O. Improved IL-2 immunotherapy by selective stimulation of IL-2 receptors on lymphocytes and endothelial cells. Proc Natl Acad Sci U S A. 2010; 107 (26):11906–11911. [PubMed: 20547866]
16. Letourneau S, et al. IL-2/anti-IL-2 antibody complexes show strong biological activity by avoiding interaction with IL-2 receptor alpha subunit CD25. Proc Natl Acad Sci U S A. 107(5):2171–2176. [PubMed: 20133862]
17. Rosenberg SA, Mule JJ, Spiess PJ, Reichert CM, Schwarz SL. Regression of established pulmonary metastases and subcutaneous tumor mediated by the systemic administration of high-dose recombinant interleukin 2. J Exp Med. 1985; 161 (5):1169–1188. [PubMed: 3886826]
18. Rao BM, Driver I, Lauffenburger DA, Wittrup KD. Interleukin 2 (IL-2) variants engineered for increased IL-2 receptor alpha-subunit affinity exhibit increased potency arising from a cell surface ligand reservoir effect. Mol Pharmacol. 2004; 66 (4):864–869. [PubMed: 15385640]
19. McCoy AJ, et al. Phaser crystallographic software. J Appl Crystallogr. 2007; 40 (Pt 4):658–674. [PubMed: 19461840]
20. Adams PD, et al. PHENIX: building new software for automated crystallographic structure determination. Acta Crystallogr D Biol Crystallogr. 2002; 58 (Pt 11):1948–1954. [PubMed: 12393927]
21. Emsley P, Cowtan K. Coot: model-building tools for molecular graphics. Acta Crystallogr D Biol Crystallogr. 2004; 60 (Pt 12 Pt 1):2126–2132. [PubMed: 15572765]

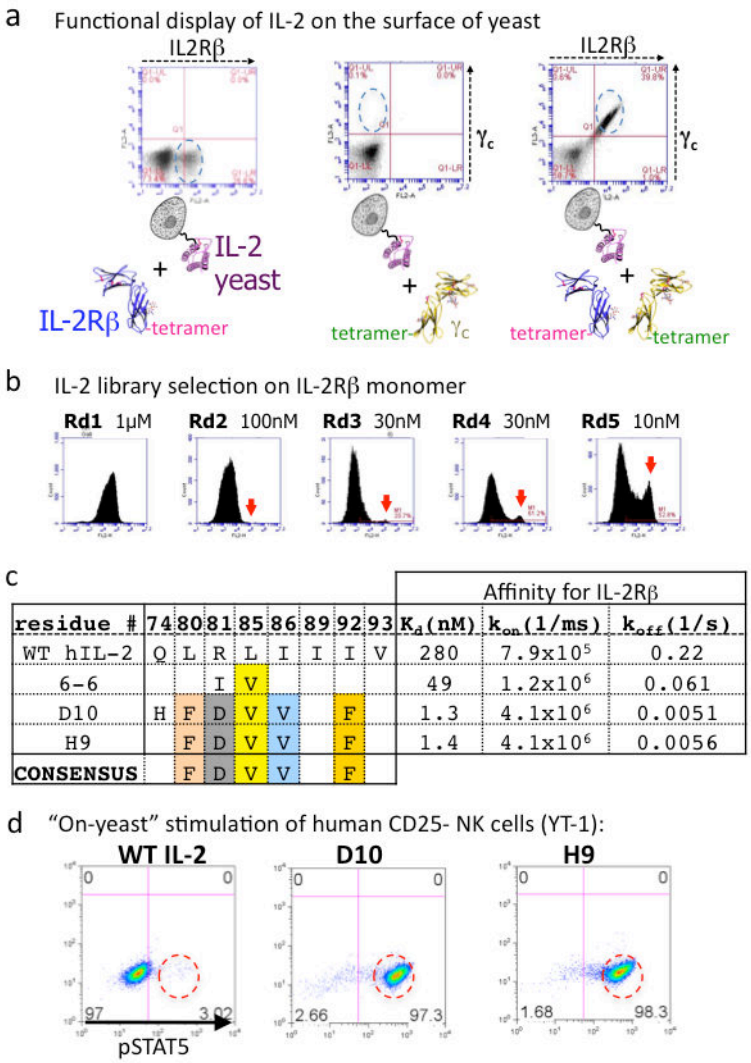

									Affinity for IL-2Rβ		
residue #	74	80	81	85	86	89	92	93	K_d(nM)	k_{on}(1/ms)	k_{off}(1/s)
WT hIL-2	Q	L	R	L	I	I	I	V	280	$7.9x10^5$	0.22
6-6			I	V					49	$1.2x10^6$	0.061
D10	H	F	D	V	V		F		1.3	$4.1x10^6$	0.0051
H9		F	D	V	V		F		1.4	$4.1x10^6$	0.0056
CONSENSUS		F	D	V	V		F				

Figure 1. *In vitro* evolution of human IL-2 variants with high affinity for IL-2Rβ

a, IL-2 displayed on yeast recapitulates cooperative receptor-binding activity. As measured by flow cytometry, IL-2 binds weakly to IL-2Rβ (left panel), undetectably to γ_c (middle panel), and cooperatively forms the IL-2Rβ/γ_c heterodimer (right panel). **b**, Enrichment of IL-2 variants on yeast by selection with progressively lower concentrations of IL-2Rβ. Arrows indicate an emerging population of high affinity IL-2Rβ binders (see also Supplementary Fig. 2). **c**, Sequences and affinities for IL-2Rβ of selected mutants from the first (mutant 6-6) and second (mutants D10 and H9) generation libraries (see Supplementary Fig. 3 for an extended table). **d**, On-yeast stimulation of YT-1 cells (human NK cell line) by wild-type (WT) IL-2-yeast and high affinity variants (super-2s) (see also Supplementary Fig. 4).

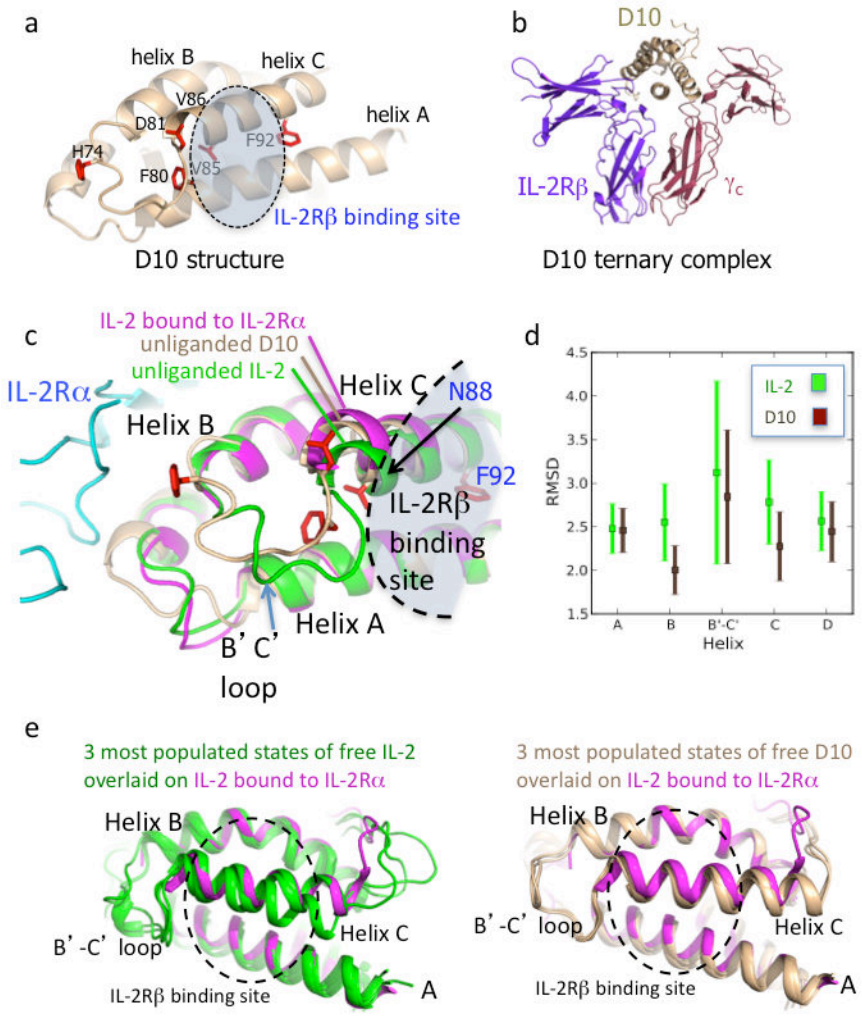

Figure 2. Basis of affinity enhancement for IL-2Rβ from structural and molecular dynamics characterization of D10 super-2

a, Crystal structure of the D10 super-2 at 3.1 Å with mutated residues in red (see also Supplementary Table 1 and Supplementary Fig. 7a). **b**, D10 in complex with human IL-2Rβ and γ_c preserves the WT receptor dimer geometry (see also Supplementary Fig. 7b). **c**, The unliganded D10 super-2 helix C (brown), moves towards its hydrophobic core compared to unliganded WT IL-2 (green, PDBID 3INK). This helix C position is more similar to that of helix C in IL-2 bound to IL-2Rα (purple, PDBID 1Z92) (see also Supplementary Fig. 8). **d**, A 40ns MD simulation shows a reduction of the average RMSD for the B and C helices, and the B-C loop in D10 versus IL-2 (see also Supplementary Fig. 8c). Error bars represent the standard error of the RMSD. **e**, Helix C in IL-2 (green, left panel) drifts during the MD simulation more than super-2 D10 (brown, right panel) when compared to IL-2 bound to IL-2Rα (purple).

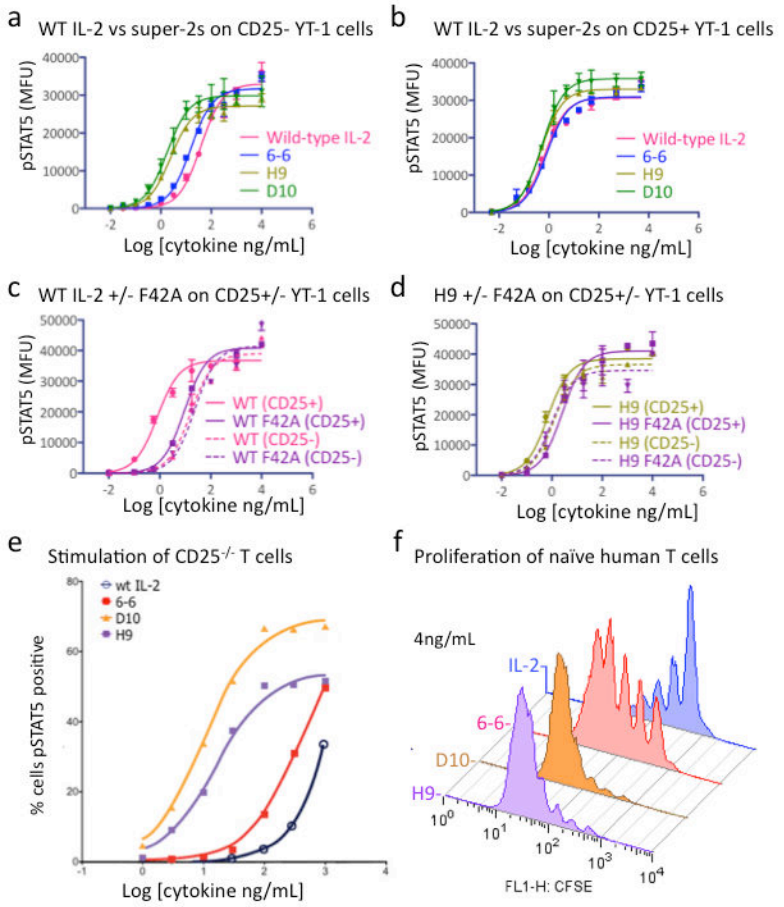

Figure 3. Functional properties of super-2 on human NK cells *in vitro*

Dose-response curves of STAT5 phosphorylation on (**a**) CD25^{-} and (**b**) CD25+ YT-1 cells with WT IL-2 and three super-2s. **c**, Dose-response curves of STAT5 phosphorylation on CD25^{+} (solid curve) and CD25^{-}(dashed curve) YT-1 cells with WT IL-2 (pink curves) and IL-2-F42A mutation (purple curves). **d**, Dose-response curves of STAT5 phosphorylation on CD25^{+} (solid curve) and CD25^{-}(dashed curve) YT-1 cells with H9 (green curves) and H9-F42A mutation (purple curves). **e**, Super-2s have superior potency over IL-2 on T cells derived from CD25$^{-/-}$ mice as demonstrated by dose-response curves for STAT5 phosphorylation on T cells demonstrating that potency correlates with IL-2Rβ affinity (see also Supplementary Fig. 10). **f**, Proliferation of human naïve CD4^{+} T cell (CD25^{low}) reveals similar potency profiles as seen with CD25$^{-/-}$ T cells. Proliferation was measured by CFSE dilution on day 5 (see also Supplementary Fig. 10). Error bars in **a–d** represent SEM of mean fluorescence units for each sample at the indicated cytokine concentration.

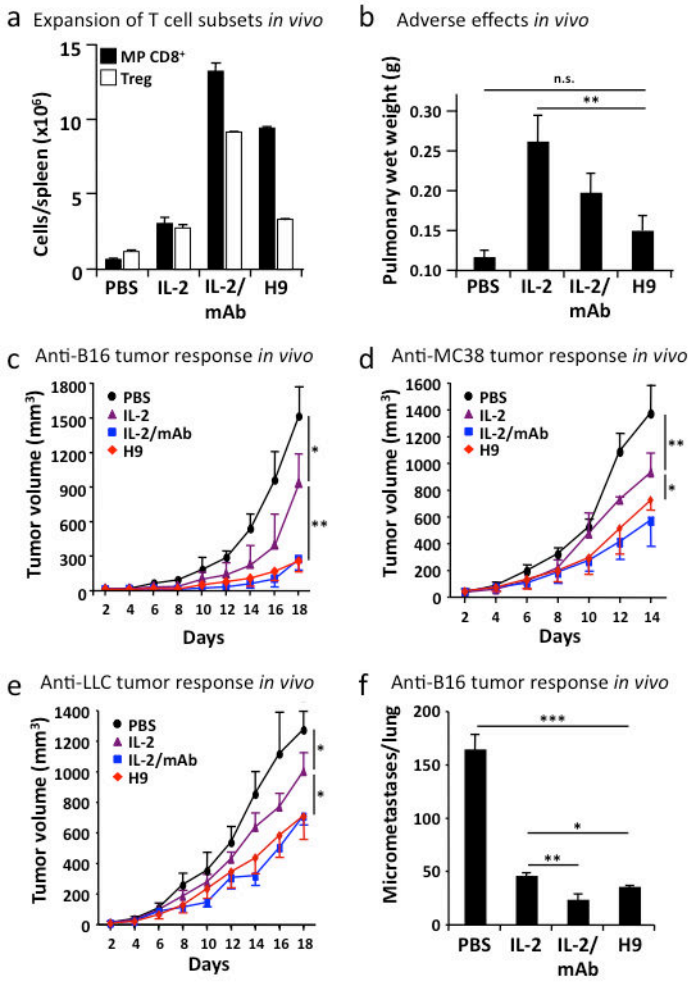

Figure 4. Functional and anti-tumor activities of super-2 *in vivo*

a, Total cell counts of host $CD3^+$ $CD8^+$ $CD44^{high}$ memory-phenotype T cells (MP $CD8^+$, closed bars), and host $CD3^+$ $CD4^+$ $CD25^{high}$ T cells (Treg, open bars) was determined in the spleens of mice receiving either PBS, 20 μg IL-2, 1.5 μg IL-2/anti-IL-2 mAb complexes (IL-2/mAb), or 20 μg H9 (see also Supplementary Fig. 14). **b**, Pulmonary edema (pulmonary wet weight) served to assess adverse toxic effects following IL-2 treatment, and was determined by weighing lungs before and after drying. **c–f**, C57BL/6 mice (n=3–4 mice/group) were injected either subcutaneously with 10^6 B16F10 melanoma cells (B16, **c**), 2.5×10^6 murine colon carcinoma 38 (MC38, **d**), 10^6 Lewis lung carcinoma (LLC, **e**), or mice received 3×10^5 B16F10 melanoma cells intravenously (B16, **f**), followed by daily injections of either PBS, 20 μg IL-2, 1.5 μg IL-2/mAb complexes, or 20 μg H9 for five days once subcutaneous tumor nodules became visible and palpable or from day three on for intravenously-injected tumors (see also Supplementary Fig. 15). Shown is mean tumor volume in mm^3 (+/− SD) vs. time upon tumor inoculation. Error bars represent SEM. *P* values refer to comparisons of WT with the other treatment modalities. *, $p<0.05$; **, $p<0.01$; ***, $p<0.001$.